



## Assessment of the ERA-Interim reanalysis winds using high-altitude stratospheric balloons

Fabrice Duruisseau, Nathalie Huret, Alice Andral, Claude Camy-Peyret

### ► To cite this version:

Fabrice Duruisseau, Nathalie Huret, Alice Andral, Claude Camy-Peyret. Assessment of the ERA-Interim reanalysis winds using high-altitude stratospheric balloons. *Journal of the Atmospheric Sciences*, 2017, 74 (6), pp.2065-2080. 10.1175/JAS-D-16-0137.1 . insu-01527457

HAL Id: insu-01527457

<https://insu.hal.science/insu-01527457>

Submitted on 19 Oct 2017

**HAL** is a multi-disciplinary open access archive for the deposit and dissemination of scientific research documents, whether they are published or not. The documents may come from teaching and research institutions in France or abroad, or from public or private research centers.

L'archive ouverte pluridisciplinaire **HAL**, est destinée au dépôt et à la diffusion de documents scientifiques de niveau recherche, publiés ou non, émanant des établissements d'enseignement et de recherche français ou étrangers, des laboratoires publics ou privés.

# Assessment of the ERA-Interim reanalysis winds using high-altitude stratospheric balloons

Fabrice DURUISSEAU<sup>1</sup> and Nathalie HURET

5 Laboratoire de Physique et Chimie de l'Environnement et de l'Espace, Centre National de  
6 la Recherche Scientifique and Université d'Orléans  
7 Orléans, France

Aless ANDRAI

10 Centre National d'Etudes Spatiales

Toulouse, France

13 Claude CAMY-PEYRET

14 Institut Pierre Simon Laplace (IPSL), UPMC/UVSQ  
15 Paris, France

<sup>1</sup> Corresponding author: Fabrice Duruisseau, CNRM/GMAP, 42 Av. G. Coriolis, 31057 TOULOUSE, FRANCE. E-mail: [fabrice.duruisseau@meteo.fr](mailto:fabrice.duruisseau@meteo.fr)

17

## ABSTRACT

18 This study focuses on the ability of the ECMWF ERA-Interim reanalysis to represent wind  
19 variability in the middle atmosphere. The originality of the proposed approach is that wind  
20 measurements are deduced from the trajectories of Zero Pressure Balloons that can reach  
21 high stratospheric altitudes. These balloons are mainly used to carry large scientific  
22 payloads. The trajectories of balloons launched above Esrange (Sweden) and Teresina  
23 (Brazil) from 2000 to 2011 were used to deduce zonal and meridional wind components  
24 (by considering the balloon as a perfect tracer at high altitude). Collected data cover  
25 several dynamical conditions associated with the winter and summer polar seasons and  
26 West and East Phases of the quasi-biennial oscillation at the equator. Systematic  
27 comparisons between measurements and ERA-Interim reanalysis data were performed  
28 for the two horizontal wind components, as well as wind speed and wind direction in the  
29 [100; 2] hPa pressure range to deduce biases between the model and balloon  
30 measurements as a function of altitude.

31 Results show that whatever the location and the geophysical conditions considered,  
32 biases between ERA-Interim and balloon wind measurements increase as a function of  
33 altitude. The standard deviation of the model/observation wind differences can attain  
34 more than  $5 \text{ m s}^{-1}$  at high altitude ( $P < 20 \text{ hPa}$ ). A systematic ERA-Interim underestimation  
35 of the wind speed is observed and large biases are highlighted especially for equatorial  
36 flights.

37

38 **1. Introduction**

39 The current computing performances of numerical weather prediction (NWP) and climate  
40 research models provide higher and higher spatial as well as temporal resolution. To  
41 improve accuracy, the models need to assimilate more and more measurements with  
42 greater precision (Dee et al. 2011). This is possible due to progress in measurement  
43 techniques and instrumentation. Wind measurements come from weather stations,  
44 radiosonde balloons, pilot balloons, aircraft meteorological reports, wind profilers and  
45 satellite imagery through atmospheric motion vectors (Borde et al. 2014, Borde et al.  
46 2016). The troposphere is well monitored because of its easier access and its direct impact  
47 on human activities. The stratosphere, however, suffers from a clear lack of *in situ* wind  
48 measurements, even though it has been shown that tropospheric weather can be  
49 influenced by large scale dynamical structures occurring in the middle atmosphere such  
50 as: i) the polar vortex (Baldwin and Dunkerton 2001; Thompson et al. 2002; Charlton et  
51 al. 2003; Charron et al. 2012); ii) sudden stratospheric warmings (SSW) (Charlton et al.  
52 2003; Charron et al. 2012; Sigmond et al. 2013; Kuttippurath and Nikulin 2012); iii) the  
53 quasi-biennial oscillation (QBO) (Thompson et al. 2002; Gerber et al. 2010). The study and  
54 numerical modelling of the stratosphere is therefore becoming an important issue for  
55 NWP centres, with numerical models considering an increasing number of horizontal grid  
56 points and vertical levels, and for most of them a model top at 0.01 hPa. They also benefit  
57 from the development of new assimilation schemes and an increase in computing  
58 facilities. Reanalysed winds result from the model internal dynamics and from assimilated  
59 observations, which can be wind observations or mass-related quantities (e.g.  
60 temperature) in places where there is a balance between the mass and wind fields (as in  
61 the extratropics).

62 Most of the wind measurements in the upper troposphere and in the lower stratosphere  
63 are performed with radiosondes that are the only *in situ* measurements in the  
64 stratosphere, but radiosondes generally burst below 30 km (around 10 hPa). Other  
65 techniques can be used to probe the atmospheric wind at high altitude (stratosphere and

mesosphere) by remote sensing. Infrasound technology (Le Pichon et al. 2005) gives relevant information on gravity waves (Blanc et al. 2014). Doppler LIDAR measurements provide measurements up to 60 km but only in some locations over the world (Hauchecorne and Chanin 1980; Chanin et al. 1989). Recently a microwave wind radiometer (WIRA) was developed at Bern University capable of measuring wind between 25 and 70 km (Rufenacht et al. 2012). Le Pichon et al. (2015) have shown large discrepancies between WIRA observations and the European Centre for Medium-Range Weather Forecasts (ECMWF) operational model, ERA-Interim and MERRA reanalyses for both temperature and wind fields above 40 km altitude. Their study highlighted the increase in wind biases as a function of altitude. The last three techniques listed provide relevant wind information by remote sensing up to the mesosphere but with a smaller vertical resolution than *in situ* measurements. New infrastructures aiming to combine these different instrumentations are emerging (ARISE project, <http://arise-project.eu/>). Satellite measurements able to probe the temperature inside the stratosphere are also expanding, such as AMSU (Kidder and von der Haar 1995) and IASI (Smith et al. 2012).

Baron et al. (2013) summarized wind measurements from space available in the middle atmosphere since HRDI measurements in 1991 (Ortland et al. 1996) to the future European Space Agency (ESA) Mission AEOLUS (Straume-Lindner et al. 2007). In their study they report the altitude range of the different measurements as well as their precision which is between  $3 \text{ m s}^{-1}$  and  $10 \text{ m s}^{-1}$  in the altitude range [10; 40] km. The vertical resolution of these wind measurements is 5-7 km. They show that using the passive microwave radiometer SMILES instrument operated on the International Space Station (ISS), good agreement between the horizontal wind components and the ECMWF analyses is reached in most of the stratosphere except for the zonal winds over the equator with a mean difference from  $5 \text{ m s}^{-1}$  to  $-10 \text{ m s}^{-1}$ , whereas in the mesosphere differences greater than  $20 \text{ m s}^{-1}$  are observed in SMILES and ECMWF zonal winds, especially in the tropics.

The present study is based on observations collected during balloon flights performed by the CNES (Centre National d'Etudes Spatiales) to investigate *in situ* the stratosphere. The

95 CNES operates several types of balloons: the Zero Pressure Balloon or ZPB (Durry and  
96 Hauchecorne 2005; Huret et al. 2006; Wetzel et al. 2013), the Super-Pressure Balloon or  
97 SPB (Vial et al. 2011; Hertzog et al. 2004; Hertzog et al. 2006; Knudsen et al. 2006;  
98 Christensen et al. 2007; Vincent and Hertzog 2014; Podglajen et al. 2014), and the Infra-  
99 Red Montgolfier Balloon (Knudsen et al. 2002; Knudsen et al. 2006; Christensen et al.  
100 2007).

101 ZPBs carry heavy scientific payloads (several hundred kg to one ton) to study the  
102 atmosphere (chemical composition and its dynamics), aeronomy or astrophysics. The  
103 flight duration is from several hours to a few days or a few weeks. They have been  
104 intensively used to validate satellite measurements (ENVISAT, ODIN, ILAS, etc.). They can  
105 attain high stratospheric altitudes up to 40 km.

106 SPBs are used in the UT-LS (Upper Troposphere-Low Stratosphere) for long duration flights  
107 (1-3 months) on isopycnic surfaces. Several studies (Hertzog et al. 2004; Knudsen et al.  
108 2006; Christensen et al. 2007; Boccara et al. 2008) have reported substantial differences  
109 between simulated balloon trajectories with analysed winds and real trajectories using  
110 SPBs in the upper troposphere and low stratosphere (UT-LS), with differences of a  
111 thousand kilometres between the forecast trajectory and the real one at mid and high  
112 latitudes after a few days of flight. In equatorial regions this difference is higher and can  
113 attain 10 000 km after ten days of trajectory forecast (Podglajen et al. 2014).

114 The balloon trajectory is driven by the wind, and balloons can be considered as good  
115 tracers if the vertical speed is not too high and if measurements of the balloon location  
116 are sufficiently accurate (Alexander et al. 1996).

117 In the present study we used ZPB (operated by CNES) trajectories in the 2000-2011 period  
118 in order to retrieve the wind components (zonal i.e. u and meridional i.e. v), the wind  
119 speed (FF) or wind direction (DD) and compare them with the ERA-Interim data. These *in*  
120 *situ* wind measurements allowed us to study the ability of ERA-Interim to represent the  
121 dynamics of the stratosphere up to 2 hPa above two balloon launch bases (Esrang  
122 (67.9°N., 21.1°E) in Sweden and Teresina (5.1°S., 42.9°W) in Brazil) in several dynamical  
123 conditions (winter and summer polar seasons, West and East phases of the quasi-biennial  
124 oscillation at the Equator). It should be noted that the ERA-Interim reanalysis process  
125 assimilates much less wind data in the stratosphere than in the troposphere (Dee et al.  
126 2011).

127 In the present paper we first describe the balloon wind measurements and the retrieval  
128 method used as well as the methodology developed for comparing with ERA-Interim  
129 reanalyses (Dee et al. 2011). We then assess the wind biases for each dynamical condition  
130 and we conclude by discussing the results in terms of specific processes/conditions which  
131 could explain the biases obtained as well as the methodology used.

132

133 **2. Data and methodology**

134 *a. Zero Pressure Balloon wind measurements*

135 The typical duration of ZPB flights operated by CNES is from 6 hours to a few days. Each  
136 flight profile is driven by scientific objectives depending on the payload, with four phases:  
137 (1) balloon ascent at typically  $5 \text{ m s}^{-1}$ , (2) ceiling where the balloon is in equilibrium with  
138 the surrounding air thus the pressure level is stable (except for slow variations due to  
139 thermal effects induced by the diurnal cycle), (3) slow descent with a vertical speed that  
140 can be adjusted between  $1 \text{ m s}^{-1}$  and  $5 \text{ m s}^{-1}$ , (4) rapid descent of the payload under  
141 parachutes down to the ground after balloon-payload separation (vertical speed can  
142 exceed  $20 \text{ m s}^{-1}$ ).

143 In our study the slow phase of ascent, the ceiling and the slow descent (if present) were  
144 used to deduce the zonal wind component ( $u$ ) and the meridional wind component ( $v$ )  
145 from the balloon trajectory. The rapid descent cannot be used due to its high vertical  
146 speed. In this study we assume that the balloon is a perfect passive tracer for horizontal  
147 wind.

148 For each flight we retrieved  $u$  and  $v$  from the GPS (Global Positioning System) position  
149 (longitude, latitude, altitude) of the balloon recorded every 10 s using a centred difference  
150 with two points separated by 10 time steps (100 s). This makes it possible to filter out the  
151 high frequencies generated by pendulum oscillations. The flight chain is between 100 m  
152 and 200 m long and thus (considering a simple gravity pendulum in the small-angle  
153 approximation) the oscillation period is between 20 s and 30 s. For ZPBs the time duration  
154 of the ceiling can attain 1 day. During this phase at float a large number of measurements

155 are recorded at a roughly constant pressure. In order to avoid oversampling during the  
156 ceiling we downsampled the measurements with a time step of 15 minutes (the same  
157 sampling was used by Hertzog et al. (2004) with SPB trajectories).

158 From horizontal GPS coordinates, the accuracy of the balloon payload location is better  
159 than 10 m in the horizontal. Uncertainty due to GPS accuracy on the horizontal component  
160 is therefore  $0.2 \text{ m s}^{-1}$ . The pressure uncertainty is about 0.5 hPa (capacitive transducer  
161 probe). Such an uncertainty is too high for our study in the stratosphere because it  
162 corresponds to an error higher than several hundred meters at 10 hPa. The GPS altitude  
163 with an accuracy of 20 m was therefore used. Because the GPS antenna is not located at  
164 the centre of balloon drag, to obtain the altitude of the wind measurement points we  
165 added an offset to the GPS altitude. It corresponds to the distance between the GPS  
166 module and the mean position of the helium bubble centre, including the flight chain  
167 length. Because during the ascent of the balloon the helium bubble volume varies due to  
168 a pressure decrease, its centre is located at the geometric balloon centre only during the  
169 ceiling. Knowing the volume of helium for each flight at ground we calculate the position  
170 of the helium bubble centre at 200 hPa assuming that the volume occupied by the gas is  
171 spherical. Then we add to the balloon radius the half distance between the geometric  
172 balloon centre (at the ceiling the balloon is completely inflated) and the helium bubble  
173 centre at 200 hPa. For balloons of  $400\,000 \text{ m}^3$  and  $12\,000 \text{ m}^3$ , these offsets are  
174 respectively 110 m and 78 m. The vertical uncertainty due to the displacement of the  
175 helium bubble centre is equal to these half distances ( $\pm 37 \text{ m}$  and  $\pm 22 \text{ m}$  respectively).  
176 Adding the GPS accuracy to the maximum value of the vertical uncertainty (for a 400 000

177  $\text{m}^3$  balloon), this gives an error on the altitude of the measurement points of  $\pm 57 \text{ m}$  for all  
178 flights. It includes the accuracy of the GPS altitude and the variation in the location of the  
179 helium bubble centre during the ascent.

180 Wind measurements were retrieved from flights above Esrange (Sweden,  $67.9^\circ\text{N}.$ ,  $21.1^\circ\text{E}$ )  
181 and Teresina (Brazil,  $5.1^\circ\text{S}.$ ,  $42.9^\circ\text{W}.$ ), delivering a unique source of wind measurements in  
182 the stratosphere. They are shown in Figure 1 for both zonal and meridional wind  
183 components (77084 points).

184 We distinguish winter and summer circulation for polar flights, and the QBO phase for  
185 equatorial flights. The winter polar circulation (49 flights from Esrange in December,  
186 January and February) is characterized by westerly circulation with strong zonal winds up  
187 to  $60 \text{ m s}^{-1}$  corresponding to the edge of the polar vortex i.e. polar night jet (Krishnamurti  
188 1959; Kuroda and Kodera 2001; Hitchcock et al. 2013). During polar summer (22 flights in  
189 June, July and August) the easterly circulation is less intense.

190 For flights above Teresina (May, June and July) we observe westerly winds (QBO West) for  
191 the seven flights in 2008 in the range [20; 34] km, and easterly winds (QBO East) for the  
192 twelve flights in 2005 in the range [22; 34] km. The maximum value of the vertical  
193 gradients of both wind components is  $15 \text{ m s}^{-1} \text{ km}^{-1}$  at high level for equatorial flights.

194 The meridional wind velocities for polar summer and QBO East and West phases do not  
195 exceed  $10 \text{ m s}^{-1}$  in absolute values. For polar winter the meridional component is more  
196 variable and can attain  $50 \text{ m s}^{-1}$  in absolute values for some flights, likely caused by strong  
197 planetary waves.

198 An added value of this dataset is that wind measurements are available above 30 km in  
199 the stratosphere, while studies using meteorological radiosondes are limited to  
200 measurements below 30 km (Houchi et al. 2010; Moffat-Griffin et al. 2011 for example).

201

202 *b. ECMWF ERA-Interim reanalysis data*

203 The ECMWF model is one of the best NWP models, producing analysis and reanalysis data  
204 at a global scale (Martineau and Son 2010; Jakobson et al. 2012). The current operational  
205 model or Integrated Forecast System (IFS) has been used systematically for trajectory  
206 forecasting during CNES balloon campaigns. Over the last 20 years the IFS model has been  
207 regularly updated to include new parameterizations, data assimilation and a larger  
208 number of horizontal grid points and vertical levels. To compare with our measurements  
209 obtained from 2000 to 2011 we need results coming from the same “stable” model to  
210 perform model/balloon comparisons. We therefore chose to perform a systematic  
211 comparison with the ERA-Interim reanalyses (Dee et al. 2011) as the underlying dynamics  
212 of the model did not change over the reanalysis period.

213 The main assimilation sources in the stratosphere are radiance observations. By using the  
214 TOMCAT chemical transport model (Chipperfield, 2006) in ERA-Interim, an improvement  
215 was obtained compared to the ERA-40 reanalyses (Uppala et al. 2005) which encountered  
216 difficulties in representing the Brewer-Dobson circulation (Dee and Uppala. 2008). Dee et  
217 al. (2011) present a table summarizing the number of wind measurements and their  
218 quality, used for ERA-40 and ERA-Interim reanalysis (their table III). Their numbers are the  
219 same in 1995, but in 2006 more wind measurements were assimilated by the model.

220 However above 100 hPa (i.e. in the stratosphere) only a few wind measurements are  
221 available compared to the troposphere.

222 We used the ERA-Interim wind, pressure, temperature and geopotential height outputs  
223 on the 60 model levels with a horizontal resolution of  $0.75^\circ \times 0.75^\circ$  in latitude and  
224 longitude and a time step of 6 hours (for details see IFS documentation  
225 [http://www.ecmwf.int/sites/default/files/IFS\\_CY40R1\\_Part3.pdf](http://www.ecmwf.int/sites/default/files/IFS_CY40R1_Part3.pdf)).

226 Spatio-temporal interpolations were performed for each wind measurement by  
227 considering 3 latitude points, 3 longitude points, 2 vertical levels and 3 time steps.

228 Horizontal and time interpolations were quadratic whereas the vertical interpolation was  
229 linear. For the vertical interpolation, the geopotential height and the GPS altitude were  
230 used due to the poor precision of the operational pressure measurements on board ZPBs.

231 The error associated with the uncertainty in GPS vertical positions when we perform the  
232 vertical interpolation of reanalyzed winds depends on the wind vertical gradient which  
233 reaches  $15 \text{ m s}^{-1} \text{ km}^{-1}$  combined with the uncertainty on the altitude of the measurement  
234 points ( $\pm 57 \text{ m}$ , detailed in part 2.a). We estimated that the interpolation error was  $\pm 0.85$   
235  $\text{m s}^{-1}$ . The estimated uncertainty on individual horizontal wind measurements including  
236 the accuracies of the GPS on the horizontal axis, vertical axis, uncertainty on the position  
237 of the helium bubble centre and interpolation is therefore  $\pm 1.05 \text{ m s}^{-1}$ . We consider an  
238 additional source of error for equatorial flights due to the strong vertical wind gradient. In  
239 that case the GPS could be not aligned with the helium bubble centre. If we consider an  
240 angle of  $\pm 22.5^\circ$  between the flight chain and the vertical axis this induces a shift of roughly  
241  $\pm 23 \text{ m}$  on the horizontal axis and  $\pm 10 \text{ m}$  on the vertical axis. This could induce an

242 additional uncertainty of  $\pm 0.7 \text{ m s}^{-1}$ . For equatorial flights we then consider an estimated  
243 uncertainty on individual wind measurements of  $\pm 1.75 \text{ m s}^{-1}$  reported in each Figure.

244

245 *c. Methodology*

246 The wind biases (i.e. the mean of the difference between model and measurements) were  
247 calculated in pressure bins with two different pressure interval widths with a constant  
248 offset of the interval centre in log pressure between 100 hPa to 2 hPa (5 hPa at 100 hPa).

249 The two pressure interval widths are shown in Figure 2: Large Pressure Intervals (hereafter  
250 LPI) in red and Small Pressure Intervals (hereafter SPI) in green. Vertical levels of ERA-  
251 Interim are shown in blue in Figure 2.

252 More details can be found in Huret et al. (2015). The intervals correspond to a vertical  
253 thickness from 3.3 km at 100 hPa to 3.7 km at 5 hPa for SPI, and from 8.8 km at 100 hPa  
254 to 10.3 km at 5hPa for LPI. Biases calculated using LPI could then be compared to those  
255 from Le Pichon et al. (2014) with the WIRA Instrument which provides wind  
256 measurements in a layer with an 8 km thickness (between 30 and 38 km), or those from  
257 Baron et al. (2013) with the SMILES instrument on the ISS with a vertical resolution of 5  
258 km to 7 km from 35 km to 70 km.

259 The number of measurement points within each interval is almost constant as a function  
260 of the mean pressure up to intervals centred at 5 hPa. This allowed us to compare our  
261 results with those obtained in the different intervals i.e. to analyse the results as a function  
262 of altitude. The order of magnitude of the number of points in each LPI is 10000, 6000

263 and 5000 for respectively polar winter, polar summer and QBO east and west. For SPI, the  
264 number of points is lower with 4000, 2500 and 2000. At high altitude when the mean  
265 pressure is less than 5 hPa, the number of points strongly decreases. The number of points  
266 for equatorial flights is smaller than for polar flights due to the limited number of  
267 campaigns in equatorial regions (2005 and 2008).

268 For each interval we calculated the bias, the standard deviation, the skewness, and the  
269 kurtosis for both wind components. We also calculated the standard error on the bias  
270 (standard deviation divided by the square root of the number of points) to ensure that  
271 our results were statistically significant. It is important to note also that because numerous  
272 independent flights were used, the wind measurements obtained are independent.

273

### 274 **3. Results**

275 In this section we analyse the biases obtained in the four geophysical conditions (polar  
276 winter, polar summer, QBO east and QBO west).

277

#### 278 **3.1 Wind biases above the Esrange launch base**

##### 279 *a. Winter condition*

280 The biases in the zonal component ( $u$ ) (Figure 3) are small between  $-0.2 \text{ m s}^{-1}$  and  $+0.2 \text{ m}$   
281  $\text{s}^{-1}$  in the pressure range [100; 10] hPa for both LPI and SPI.. In the [10; 5] hPa pressure  
282 range, the  $u$  biases increase slightly to reach  $-1.2 \text{ m s}^{-1}$  at the mean pressure of 5.95 hPa  
283 for LPI and  $-1.5 \text{ m s}^{-1}$  for SPI at the mean pressure of 6.60 hPa.

284 The values of the standard deviations increase with the altitude and are roughly two times  
285 higher at 5 hPa mean pressure than at 100 hPa ( $4.6 \text{ m s}^{-1}$  compared to  $2.3 \text{ m s}^{-1}$  for both  
286 LPI and SPI). For each altitude they are greater than the estimated wind uncertainty. In  
287 each interval the standard errors are less than  $0.1 \text{ m s}^{-1}$  for both LPI and SPI. The bias  
288 values of the meridional component ( $v$ ) are small. They remain in the range [-0.1; 0.7]  $\text{m}$   
289  $\text{s}^{-1}$  for LPIs and in the range [-0.4; 1.1]  $\text{m s}^{-1}$  for SPIs. The standard deviations are constant  
290 ( $\sim 2.3 \text{ m s}^{-1}$ ) in the UT-LS up to 50 hPa and then increase up to 5 hPa with a value of almost  
291  $6 \text{ m s}^{-1}$ . They are larger than the estimated wind uncertainty. The standard errors are less  
292 than  $0.1 \text{ m s}^{-1}$  for LPI and  $0.2 \text{ m s}^{-1}$  for SPI.

293 At all levels for both wind components the standard deviations are greater than the  
294 individual measurement uncertainty for LPI and SPI. They increase with altitude,  
295 highlighting that the modelled winds reproduce less and less the variability of the  
296 observed winds. Baron et al. (2013) compared SMILES measurements and ECMWF  
297 analyses. During the 2009/2010 winter they report meridional and zonal bias values lower  
298 than  $\pm 2 \text{ m s}^{-1}$  in the stratosphere (above 10 hPa), which does not disagree with our study  
299 but they obtain very high standard deviations ( $13 \text{ m s}^{-1}$ ) compared to us. The processes  
300 responsible for wind flow perturbations during winter in polar regions are those  
301 associated with Sudden Stratospheric Warming (SSW) events at large scale and gravity  
302 wave activity at small scales. The major SSW event occurring in winter 2009/2010  
303 (Kuttippurath et al., 2012) is associated with a Polar Jet Oscillation (PJO) and vortex split  
304 (Ern et al., 2016). The latter study analysing gravity activity reported that such a  
305 combination of major SSW and PJO leads to the enhancement of gravity wave activity.

306 The propagation conditions are improved and the activity of gravity wave sources is  
307 stronger. Mountain waves are more excited and jet-generated gravity wave sources more  
308 active. This could explain the high standard deviation reported by Baron et al. (2013) for  
309 the 2009/2010 winter.

310 In our study the increase in the standard deviations as a function of altitude can also be  
311 explained by gravity wave activity given that Scandinavian mountains are a hot spot for  
312 mountain waves, as has been highlighted by numerous authors working on polar  
313 stratospheric clouds (see for example Rivi  re et al., 2001; Brogniez et al., 2003; D  rnbrack  
314 et al., 2002). However our results are based on numerous winter observations (before  
315 SSW or after, winter with or without SSW) i.e. with or without strong wave activity, which  
316 probably reduces the value of standard deviations.

317 ERA-Interim slightly underestimates the zonal wind component above 10 hPa. The u  
318 biases at high altitude ([10; 5] hPa pressure range) are relatively small compared to the u  
319 mean value ( $\sim$ 40 m s $^{-1}$ ) and do not exceed 8%. The v biases are slightly larger and can  
320 reach 11% at 23 hPa. The increase in the standard deviations with altitude highlights the  
321 difficulties of ERA-Interim in representing the wind variability observed due to gravity  
322 waves at small scale and their interaction with SSW events at large scale.

323 A specific comparison was conducted between our results around 70 hPa and the previous  
324 study by Hertzog et al. (2004; hereafter referred to as H2004). H2004 compared the two  
325 wind components deduced from 6 SPB trajectories obtained in 2002 in polar vortex

326 conditions to the ECMWF operational outputs ( $0.5^\circ \times 0.5^\circ$ ). Their results combined two sets  
327 of measurements obtained in the [85.1; 82.8] hPa and [64.7; 58.6] hPa pressure ranges.

328 The pressure ranges of H2004 are included in the SPI at the mean pressure of 69.83 hPa.  
329 Figure 4 presents the histograms of differences between ERA-Interim and our wind  
330 measurements, and Table 1 summarizes the characteristics of our results and those of  
331 H2004. The histograms of differences we obtained present a Gaussian shape with small  
332 biases of  $0.1 \text{ m s}^{-1}$  and  $0.2 \text{ m s}^{-1}$  for u and v respectively. The standard deviations obtained  
333 are similar to those of H2004. Skewness and kurtosis are larger in our study (except for  
334 the zonal wind skewness). We have half as many points as H2004 and our standard error  
335 is  $0.04 \text{ m s}^{-1}$  for both u and v biases, which is smaller than the biases we obtained. Even if  
336 the biases we get are lower than the estimated uncertainty, the standard error remains  
337 lower than the biases. Moreover the standard deviations are of the same order as those  
338 of H2004. This comparison with H2004, at this specific pressure range in the low  
339 stratosphere, supports our decision to use ZPB trajectories to investigate biases between  
340 model results and measurements and the associated standard deviation.

341

342 *b. Summer conditions*

343 The zonal and meridional wind biases obtained in polar summer are presented in Figure  
344 5. For the zonal component between 100 hPa and 10 hPa, and for the meridional  
345 component up to 5 hPa, the biases are very small, close to  $0 \text{ m s}^{-1}$ , slightly positive or  
346 negative and in all cases lower than the estimated uncertainty. Above 10 hPa the zonal

347 biases increase, reaching  $-1.1 \text{ m s}^{-1}$  at 5 hPa. The standard deviations obtained are smaller  
348 than in polar winter conditions, in good agreement with climatologies of gravity waves  
349 that show the same characteristics at high altitude (Ern et al., 2011). They remain roughly  
350 constant ( $\sim 2 \text{ m s}^{-1}$ ) up to 35 hPa and then increase up to  $3.5 \text{ m s}^{-1}$  at high altitude for both  
351 wind components. The standard errors on u and v biases are less than  $0.1 \text{ m s}^{-1}$  for LPI and  
352 less than  $0.2 \text{ m s}^{-1}$  for SPI. During the summer season ERA-Interim represents both  
353 horizontal components of the wind above Esrange up to 5 hPa well. The relative u biases  
354 (considering a mean zonal wind velocity of  $-5 \text{ m s}^{-1}$  and  $-10 \text{ m s}^{-1}$ ) are less than 10% for the  
355 u component, and because the meridional wind is weak (Figure 1), the relative meridional  
356 biases can attain 30%.

357

### 358 **3.2 Wind biases above Teresina (Brazil)**

359 The dynamical conditions of the equatorial stratosphere are modulated by the QBO  
360 (Baldwin et al. 2001). In 2008 (May to June) flights took place during the westerly QBO  
361 phase whereas in 2005 (June to July) flights occurred during the easterly phase.

362

#### 363 *a. Easterly QBO phase*

364 Biases calculated for the easterly QBO phase for both wind components are shown for LPI  
365 and SPI in Figure 6 as well as standard deviations.

366 The zonal (u) wind biases obtained with LPI and SPI are mainly negative in the low levels  
367 from 100 hPa to 25 hPa, with values between  $-0.5$  and  $-3.0 \text{ m s}^{-1}$  (sometimes greater than

368 the estimated uncertainty). Above 25 hPa, the u biases obtained with SPI present large  
369 variations from negative to positive values. For SPI, local *extrema* are observed at two  
370 specific mean pressures:  $-3.1 \text{ m s}^{-1}$  at 20.39 hPa and  $9.9 \text{ m s}^{-1}$  at 9.94 hPa. For these two  
371 levels LPI give a slightly positive value of  $0.1 \text{ m s}^{-1}$  at 20.39 hPa and  $5.1 \text{ m s}^{-1}$  at 9.94 hPa  
372 which is approximatively a twofold lower value than the SPI bias. The biases are greater  
373 than the uncertainty over almost the entire vertical profile. Unlike SPI and LPI biases  
374 calculated from polar flights, those from equatorial flights present very different vertical  
375 profiles. The standard deviations for both LPI and SPI increase as a function of altitude,  
376 reaching more than  $6 \text{ m s}^{-1}$  above 7 hPa. The standard errors are less than  $0.1 \text{ m s}^{-1}$  for LPI  
377 and  $0.3 \text{ m s}^{-1}$  for SPI. They are greater than those obtained in the polar region due to the  
378 smaller number of measurement points in each pressure interval but they remain lower  
379 than the biases obtained. It is important to point out that the relative biases for u can  
380 exceed 50% in some extreme cases.

381 The meridional biases are mainly slightly negative. They are between  $-2.3$  and  $-0.4 \text{ m s}^{-1}$   
382 and between  $-3.4$  and  $0.3 \text{ m s}^{-1}$  for LPI and SPI respectively. The standard deviations  
383 present several different regions. The minimum values obtained between 30 hPa and 20  
384 hPa for SPI and LPI are  $3 \text{ m s}^{-1}$  greater than the estimated uncertainty. The standard errors  
385 are below  $0.1 \text{ m s}^{-1}$  for LPI and  $0.2 \text{ m s}^{-1}$  for SPI. As for the zonal component, the relative  
386 biases for v are large and can reach 60% (considering a meridional wind velocity of  $\sim 5 \text{ m}$   
387  $\text{s}^{-1}$ ).

388 To better understand the vertical variations in u biases we present the two histograms of  
389 differences between ERA-Interim and our measurements at 20.39 hPa and 9.94 hPa in  
390 Figure 7.

391 For a mean pressure of 9.94 hPa (Figure 7a) where SPI present a larger positive bias value  
392 than the LPI bias value, the histograms of differences show a wide scatter, with differences  
393 between model and measurements ranging from  $-10 \text{ m s}^{-1}$  to  $+21 \text{ m s}^{-1}$ . The histogram of  
394 biases for LPI presents a frequency distribution that is different from SPI with more  
395 negative bias values. This explains the shift of the biases to smaller values for LPI  
396 compared to SPI.

397 When the SPI bias is minimum and the LPI bias close to zero (at 20.39 hPa, Figure 7b) the  
398 SPI histograms present a more Gaussian shape. In that case the extent of the distribution  
399 is very different for LPI and SPI. LPI includes more positive bias values. This explains the  
400 different bias obtained for LPI and SPI: the LPI shift results in positive biases. When  
401 analysing both these histograms and the vertical distribution of u measurements (Figure  
402 1), and taking into account the fact that the vertical extents of LPIs are roughly 9.5 km, it  
403 can be seen that LPIs take into account measurement points associated with the well-  
404 established Easterly circulation as well as measurement points associated with the strong  
405 wind gradients in the vertical direction. SPI biases give information on a smaller altitude  
406 range (roughly 3.5 km) and the largest differences between ERA-Interim and wind  
407 measurements (in absolute value) are observed where the abrupt vertical transition in the  
408 zonal wind direction occurs. Hence, LPIs appear to be too large, leading to a smoothing of

409 the derived vertical bias profiles, while SPIs are more accurate to characterize the biases  
410 when wind shear exists.

411 Baron et al. (2013) showed a u bias of 5-10 m s<sup>-1</sup> at 10 hPa compared with the ECMWF  
412 analysis field over the equator. In line with our results, their v biases are small, close to  
413 zero. Their results were obtained with a vertical resolution of 5-7 km (i.e., in between the  
414 resolution of SPIs and LPIs) and our zonal biases (LPI: 7 m s<sup>-1</sup> and SPI: 10 m s<sup>-1</sup>) and  
415 meridional biases are in agreement with their findings. The biases in the present study are  
416 two or three times lower values than those of Baron et al. (2013) which refine the  
417 characterization of the biases existing between measurements using winds deduced from  
418 balloon trajectories and model outputs. Similar to ECMWF analyses, ERA-Interim seems  
419 to have difficulties capturing the altitude of the vertical transition in the zonal wind  
420 direction, or the intensity of this change.

421

422 *b. Westerly QBO phase*

423 Biases calculated for the westerly QBO phase for both wind components are shown for  
424 LPI and SPI in Figure 8 as well as the standard deviations.

425 Negative zonal wind (u) biases are obtained with LPI above 20 hPa, reaching -6 m s<sup>-1</sup> at  
426 5.11 hPa. Below this pressure, the biases are almost equal to zero or slightly positive. The  
427 u biases obtained with SPI vary widely, as for easterly QBO conditions (see section 3.2.a),  
428 with local *extrema* at specific mean pressures, namely 2 m s<sup>-1</sup> at 46.43 hPa, and -10.6 m s<sup>-</sup>  
429 <sup>1</sup> at 6.94 hPa. In the pressure range of [12.85; 28.04] hPa the biases are slightly negative,  
430 close to the estimated uncertainty, but with a smaller standard deviation of 3 m s<sup>-1</sup> than

431 below and above with roughly  $6 \text{ m s}^{-1}$ . The standard errors calculated are smaller than  $0.1$   
432  $\text{m s}^{-1}$  for LPI and  $0.2 \text{ m s}^{-1}$  for SPI. The relative u biases can exceed 40% for the extreme  
433 values. The layer [12.85; 28.04] hPa is characterized by Easterly circulation whereas above  
434 and below the circulation reverses and the standard deviations increase.

435 The biases for the meridional wind v are mainly positive in the [100; 35] hPa and [15, 5]  
436 hPa pressure ranges and negative in the [35; 15] hPa pressure range for both LPI and SPI.  
437 The values of v biases reach  $1.8 \text{ m s}^{-1}$  at 81.45 hPa for LPI,  $-3.5 \text{ m s}^{-1}$  at 23.78 hPa for SPI  
438 and  $1.9 \text{ m s}^{-1}$  at 7.31 hPa for SPI. The standard deviations are mainly between  $4 \text{ m s}^{-1}$  and  
439  $7 \text{ m s}^{-1}$ . The standard errors calculated are below  $0.8 \text{ m s}^{-1}$  for LPI and  $0.2 \text{ m s}^{-1}$  for SPI. The  
440 relative v biases can exceed 100% because the meridional circulation is weak (considering  
441 a meridional wind velocity of  $\sim 4\text{-}5 \text{ m s}^{-1}$ , see Figure 1).

442 The same behaviour as for easterly QBO conditions is observed with considerable  
443 differences between u biases for LPI and SPI, but not at the same altitude. Analysis of both  
444 vertical profiles of u biases and u measurements (Figure 1) shows that the 2 *maxima* (in  
445 absolute value) of u biases with SPI are obtained close to altitudes where the vertical u  
446 gradient is maximum; the minimum u biases with SPI are obtained in layers where vertical  
447 u gradients are minimum. Once again the greater difference between ERA-Interim and  
448 wind measurements comes from the layers where a zonal wind vertical transition in the  
449 East to West wind direction occurs. As before, the difference between LPI and SPI u biases  
450 obtained at these layers can also be explained by the histograms of distribution (not  
451 shown). LPI take into account more vertical levels, which induces a wider distribution of  
452  $u_{\text{eral}} - u_{\text{obs}}$ , thus reducing the biases when maximum bias values (in absolute value) for SPI

453 are observed and increasing the biases when minimum bias values for SPI are observed.

454 This means that if LPI intervals are used, smoothing occurs and the differences between

455 reanalysis and observations are not well captured. The standard errors calculated for SPI

456 are lower than the biases obtained, meaning that a sufficient number of data points were

457 considered to extract the information on the u biases with SPI.

458 At low levels we can compare our results to those of Podglajen et al. (2014) who estimated

459 biases with ERA-Interim by analysing two SPB flights in the [55; 65] hPa pressure range.

460 Their bias values were  $-2.7 \text{ m s}^{-1}$  and  $-0.1 \text{ m s}^{-1}$  and standard deviations of  $5.1 \text{ m s}^{-1}$  and

461  $3.8 \text{ m s}^{-1}$  for the zonal and meridional components respectively. The standard deviations

462 were similar to our results on both wind components. The biases for the zonal component

463 were below the estimated uncertainty in our study and close to  $0 \text{ m s}^{-1}$  in this range of

464 altitude.

465 As a partial conclusion on equatorial investigations, whatever the QBO phase considered

466 ERA-Interim does not fully capture the vertical structure of the zonal wind, and the

467 difference between measurements and model can attain more than  $7 \text{ m s}^{-1}$  at high

468 altitude, with a large standard deviation. Results are very sensitive to the vertical

469 resolution, with an underestimated bias value when the zonal circulation reverses

470 considering a vertical resolution close to 10 km. As a result, SMILES measurements from

471 ISS or ground-based WIRA measurements provide information about the order of

472 magnitude of the bias but do not capture the strong bias values.

473

#### 474 **4. Discussion**

475 For both zonal and meridional wind components, biases between ERA-Interim winds and  
476 wind measurements deduced from ZPB trajectories depend on the location, the season  
477 and the mean pressure. Whatever the conditions considered, the standard deviations  
478 increase with altitude. It is important to note that for each location/season no correlation  
479 was found between the vertical bias variations and the ERA-Interim levels, showing that  
480 interpolation errors can be neglected. For the different biases calculated, the standard  
481 errors are always lower than the biases obtained (even in the equatorial region with a  
482 smaller number of balloon flights, hence fewer measurements) and almost all standard  
483 deviations are greater than the estimated uncertainty. This means that even in cases of  
484 small biases, ERA-Interim seems to have difficulty representing the wind field variability  
485 in the stratosphere at high altitude.

486 We have seen that the biases obtained when considering large pressure intervals (LPI) and  
487 small pressure intervals (SPI) are similar for measurements obtained in the polar region,  
488 but that differences appear for measurements obtained in the equatorial region. The  
489 explanation for this is that in the event of a rapid change in wind direction, small pressure  
490 intervals are better suited for calculating biases. In addition, when large vertical wind  
491 gradients exist, ERA-Interim reanalyses encounter difficulty capturing these changes. The  
492 meridional component wind biases are always small but in relative value can attain 30%.  
493 In the previous part we analysed the zonal and meridional components independently,  
494 but they are not uncorrelated and it is also interesting to determine the differences  
495 between ERA-Interim and balloon measurements for wind speed (FF) and wind direction

496 (DD) (the notations FF and DD are the norms used for radiosondes (WMO, 1995)). Figure  
497 9 shows the FF and DD biases for the four geophysical conditions investigated with SPI.

498

499 **4.1 Polar flights**

500 In the polar region (winter and summer season, Figure 9a), the absolute differences  
501 between ERA-Interim and measurements in the [100; 20] hPa pressure range never  
502 exceed  $1 \text{ m s}^{-1}$ . In the [100; 50] hPa pressure range Dee et al. (2011) showed the global  
503 average of the root mean square (RMS) errors of winds from several sets of ECMWF  
504 reanalyses. This RMS can be compared with the standard deviation that we calculated on  
505 the wind speed. In the troposphere, ERA-Interim reanalyses compared to wind from  
506 radiosoundings present a RMS peak of  $\sim 5.7 \text{ m s}^{-1}$  at 250 hPa. It then decreases, reaching  
507  $4 \text{ m s}^{-1}$  at 100 hPa and  $\sim 3.2 \text{ m s}^{-1}$  at 50 hPa. The standard deviations we obtained for the  
508 wind speed for polar flights are in the same order of RMS magnitude, with values of  $3 \text{ m}$   
509  $\text{s}^{-1}$  during winter and  $1.5 \text{ m s}^{-1}$  during summer. This confirms that ERA-Interim reanalyses  
510 are robust in the low stratosphere, in good agreement with other previous studies  
511 assessing the quality of the ECMWF model in the lower stratosphere (Hertzog et al. 2004;  
512 Hertzog et al. 2006; Knudsen et al. 2006; Christensen et al. 2007; Boccara et al. 2008;  
513 Houchi et al. 2010).

514 ERA-Interim reanalyses encounter some difficulties representing wind speed at higher  
515 altitudes (above 20 hPa). The FF biases increase almost linearly, reaching  $-2.3 \text{ m s}^{-1}$  at 5  
516 hPa in winter condition and a lower value in summer condition. The ERA-Interim  
517 reanalysis underestimates slightly the wind speed above 20 hPa. This altitude corresponds

518 to the altitude rarely attained by radiosondes and consequently above 20 hPa no wind  
519 measurements can be assimilated in the model.

520 The wind direction (DD) biases can be considered as zero for polar winter conditions but  
521 with a standard deviation between 12° and 23°. In polar summer, wind direction bias can  
522 reach 20° (in absolute value) with a very strong standard deviation greater than 60°.  
523 During summer in the polar region the wind speed is small (see Figure 1) with a meridional  
524 component very close to zero. Thus, even a slight bias on u or v leads to a significant bias  
525 on DD.

526 Schroeder et al. (2009) using SABER temperature measurements evaluated the ability of  
527 the ECMWF model to resolve gravity waves at 30 km. They highlighted weaknesses of the  
528 model for representing gravity wave amplitude at high latitudes. Since most of the ZPBs  
529 attain 40 km of altitude, their trajectories reflect these small scale perturbations in the  
530 wind circulation. The increase in the standard deviations we obtained is probably due to  
531 this weakness.

532

## 533 **4.2 Equatorial flights**

534 For equatorial flights (Figure 9c and 9d), the ERA-Interim data are less accurate for both  
535 FF and DD than for polar flights. As seen in the previous parts, the values of u biases  
536 obtained for both QBO phase conditions rise with altitude and present *maxima* at  
537 different well-identified pressure levels.

538 For the easterly and westerly QBO phases (figure 9c) the wind speed is mostly  
539 underestimated by the model below 50 hPa. Above this pressure level the FF biases are

540 successively positive and negative without exceeding  $\pm 4 \text{ m s}^{-1}$  up to 15 hPa. Then for the  
541 easterly QBO phase a FF bias maximum value of  $-10.1 \text{ m s}^{-1}$  is encountered at 10 hPa. The  
542 FF standard deviation increases with altitude with a maximum value of  $5 \text{ m s}^{-1}$  at 10 hPa.  
543 The strong biases previously highlighted regarding zonal wind drive the strong biases for  
544 FF. The standard deviations are between 2 and  $5 \text{ m s}^{-1}$  in the pressure range [15; 50] hPa  
545 whereas in the low stratosphere they can attain  $6 \text{ m s}^{-1}$  and at high level more than  $12 \text{ m}$   
546  $\text{s}^{-1}$ .

547 For the westerly QBO phase DD biases oscillate between positive and negative values with  
548  $+22^\circ$  at 10 hPa and  $-30^\circ$  at 7 hPa. For the easterly QBO phase the DD biases are small (<  
549  $8^\circ$ ) up to 10 hPa but reach  $-19^\circ$  in the pressure range [9; 6.5] hPa. Low levels (below 32  
550 hPa) and high levels (above 10 hPa) are characterized by high DD standard deviations  
551 which can attain  $50^\circ$ . For both QBO phases a layer with small DD standard deviation (lower  
552 than  $10^\circ$  for the easterly QBO phase) can be seen, which corresponds to the well-  
553 established zonal circulation.

554 These results highlight that discrepancies between ERA-Interim and observed winds  
555 appear at levels where the zonal circulation reverses (reversal of wind direction). Because  
556 the vertical gradients are strong (Figure 1) a slight vertical shift in ERA-Interim can induce  
557 the strong biases highlighted here. Even if the models capture the main characteristics of  
558 the QBO (Baldwin and Gray 2005; Huang et al. 2011; Lehmann and Névir 2012), vertical  
559 dynamical structure changes in the equatorial stratosphere remain difficult to represent.  
560 Schroeder et al. (2009) show the poor representation in the ECMWF model of the waves

561 generated by convection in tropical regions. As for polar winter flights, the strong biases  
562 and standard deviations we obtained very likely denote this feature.

563

564 Above the two launch bases (polar and equatorial) and for each geophysical condition  
565 considered, the biases obtained and the standard deviations increase sharply above 20  
566 hPa (~30 km). This pressure level corresponds to the level where radiosondes burst. The  
567 lack of measurements in the high stratosphere is probably responsible for the low quality  
568 of the wind from ERA-Interim reanalyses at high altitude. Le Pichon et al. (2015) highlight  
569 an increase in biases as a function of altitude above 40 km in the Middle Atmosphere  
570 using WIRA radiometer measurements. Baron et al. (2013) showed negative bias values  
571 in the middle equatorial stratosphere on the zonal component and strong positive values  
572 in the mesosphere. Combining these findings with our study it appears that after a  
573 decrease in the wind biases above the tropopause (Dee et al. 2011), in the stratosphere  
574 (this study) up to the mesosphere (Le Pichon et al., 2015; Baron et al., 2013) the wind  
575 biases increase as well as the standard deviations.

576 The lack of wind measurements in the middle and high stratosphere means that models  
577 have to extrapolate fields in these regions or have to use the brightness temperatures  
578 measured by satellite to deduce the geostrophic wind (Rüfenacht et al. 2012; Baron et al.  
579 2013). However, this approximation breaks down due to strong wave activity especially in  
580 the tropics where the Coriolis parameter vanishes (Žagar et al. 2004; Polavarapu et al.  
581 2005, Schroeder et al. 2009) but also in the polar region as shown by Ern et al. (2016).

582

583 **5. Conclusion**

584 We have retrieved wind profiles in the stratosphere using trajectories from Zero Pressure  
585 Balloons launched in polar and equatorial regions (above Esrange in Sweden and Teresina  
586 in Brazil respectively) between 2000 and 2011. The dataset obtained provides unique *in*  
587 *situ* measurements in the mid-stratosphere up to 2 hPa. This dataset has been used to  
588 assess the ERA-Interim reanalyses through a methodology designed for studying wind  
589 biases and standard deviations as a function of pressure. In addition we consider two  
590 types of pressure intervals (with thicknesses of roughly 3.5 km and 10 km) to discuss the  
591 most suitable vertical resolution to evaluate the model results.

592 ERA-Interim reanalyses present relatively small biases for zonal and meridional wind  
593 components in the lower stratosphere during winter above the polar launch base. These  
594 results are consistent with those of Hertzog et al. (2004) obtained with ECMWF analysis  
595 at a specific pressure range for the 2002 polar vortex condition. This result attests the  
596 good quality of ERA-interim in the lower stratosphere and the slight underestimation of  
597 the zonal wind and the wind speed at high levels above 20 hPa by ERA-Interim. The  
598 standard deviations obtained increase with altitude above 20 hPa up to  $4 \text{ m s}^{-1}$  for the  
599 zonal and meridional components. They are greater for the wind speed during winter ( $6$   
600  $\text{m s}^{-1}$ ) than during summer ( $4 \text{ m s}^{-1}$ ). Wind direction in the polar summer condition appears  
601 to be considerably more variable in the observed winds than in the model with a standard  
602 deviation reaching  $80^\circ$  at 5 hPa. Because of the small wind intensity during summer, a  
603 small bias on wind components induces a strong standard deviation on wind direction.

604 The equatorial results revealed a much larger wind bias. The largest differences can  
605 exceed 50% where/when the QBO phase changes. In addition in the event of complex  
606 vertical variations in the zonal circulation such as QBO, the zonal wind biases are very  
607 sensitive to the vertical resolution considered. They are underestimated with a vertical  
608 resolution close to 10 km compared to results with a resolution close to 3.5 km. For both  
609 wind components the standard deviations are maximum at high altitude (up to  $10 \text{ m s}^{-1}$ )  
610 with altitude.

611 Our study highlights that ERA-Interim reanalyses underestimate the stratospheric wind  
612 speed whatever the geophysical conditions (albeit to a lesser degree in the polar region  
613 than in the equatorial region). As a result the variability of both wind components and  
614 wind speed observed are not well represented by ERA-Interim, especially at high levels  
615 above 20 hPa or in the QBO regime (complex vertical dynamical structure). Given that  
616 winds are modulated by gravity waves (with amplitude increasing with altitude), the  
617 model appears to encounter difficulties in representing small scales waves activities.

618

#### 619 *Acknowledgments*

620 This study was initiated by the DEDALE working group at the Centre National d'Etudes  
621 Spatiales (CNES), including links with the CSTB committee  
622 (<http://www.lmd.polytechnique.fr/cstb/>), INSU/CNRS, CNES and the ARISE project. We  
623 particularly thank Thien Lam-Trong for his initial support. This study was funded by the  
624 French Research Ministry, the Ecole Doctorale (EMSTU) of the Université d'Orléans (PhD

625 Grant). The Region Centre, the Labex VOLTAIRE (ANR-10-LABX-100-01) and SPARC/WMO  
626 (<http://www.sparc-climate.org/>) contributed to the diffusion of the results at various  
627 conferences. We thank the CNES balloon direction for providing the raw balloon trajectory  
628 files and Institut Pierre Simon Laplace (IPSL) for access to the ERA-Interim data. We thank  
629 all members of the CNES balloon launching team for their commitment during campaigns  
630 in the last two decades.

631

632

## REFERENCES

633

634 Alexander, P., J. Cornejo, and A. De la Torre, 1996: The response of an open stratospheric  
635 balloon to the presence of inertio-gravity waves. *J. Appl. Meteor.*, **35**, 60–68.

636 Baldwin, M. P. and T. J. Dunkerton, 2001: Stratospheric harbingers of anomalous weather  
637 regimes. *Science*, **294**, 581, doi: 10.1126/science.1063315.

638 Baldwin, M. P. and L. J. Gray, 2005: Tropical stratospheric zonal winds in ECMWF ERA-40  
639 reanalysis, rocketsonde data, and rawinsonde data. *Geophys. Res. Lett.*, **32**, L09806,  
640 doi:10.1029/2004GL022328.

641 Baldwin, M. P., L. J. Gray, T. J. Dunkerton, K. Hamilton, P. H. Haynes, W. J. Randel, J. R.  
642 Holton, M. J. Alexander, I. Hirota, T. Horinouchi, D. B. A. Jones, J. S. Kinnersley, C.  
643 Marquardt, K. Sato and M. Takahashi, 2001: The quasi-biennial oscillation. *Rev. Geophys.*,  
644 **39**(2), 179-229, doi:[10.1029/1999RG000073](https://doi.org/10.1029/1999RG000073).

645 Baron, P. and Coauthors, 2013: Observation of horizontal winds in the middle-atmosphere  
646 between 30° S and 55° N during the northern winter 2009–2010. *Atmos. Chem. Phys.*, **12**,  
647 32473–32513, doi:10.5194/acp-1336049-20133.

648 Blanc, E., T. Farges, A. Le Pichon, and P. Heinrich, 2014: Ten year observations of gravity  
649 waves from thunderstorms in western Africa. *J. Geophys. Res. Atmos.*, **119**, 6409–6418,  
650 doi:[10.1002/2013JD020499](https://doi.org/10.1002/2013JD020499).

651 Boccara, G., A. Hertzog, C. Basdevant and F. Vial, 2008: Accuracy of NCEP/NCAR reanalyses  
652 and ECMWF analyses in the lower stratosphere over Antarctica in 2005. *J. Geophys. Res.*,  
653 **113**, D20115, doi:10.1029/2008JD010116.

654 Borde R., O. Hautecoeur and M. Carranza, EUMETSAT Global AVHRR Wind Product, *J.*  
655 *Atmos. Oc. Tec.*, Vol. 33, No. 3, DOI: <http://dx.doi.org/10.1175/JTECH-D-15-0155.1>, 2016

656 Borde R., M. Doutriaux-Boucher, G. Dew, and M. Carranza, A Direct Link between Feature  
657 Tracking and Height Assignment of Operational EUMETSAT Atmospheric Motion Vectors,  
658 *J. Atmos. Oc. Tec.*, Vol. 31, No. 1, DOI: <http://dx.doi.org/10.1175/JTECH-D-13-00126.1>,  
659 2014

- 660 Brogniez C., N. Huret, S. Eckermann, E. D. Rivière, M. Pirre, M. Herman, J.-Y. Balois, C.  
661 Verwaerde, N. Larsen, B. Knudsen : Polar stratospheric cloud microphysical properties  
662 measured by the microRADIBAL instrument on 25 January 2000 above Esrange and  
663 modeling interpretation, *J. Geophys. Res.*, 2003, **108**, D6. doi : 10.1029/2001JD001017
- 664 Chanin, M.-L., A. Garnier, A. Hauchecorne and J. Porteneuve, 1989: A Doppler lidar for  
665 measuring winds in the middle atmosphere. *Geophys. Res. Lett.*, **16**, 1273-1276. doi:  
666 10.1029/GL016i011p01273
- 667 Charlton, A. J., A. O'Neill, D. B. Stephenson, W. A. Lahoz and M. P. Baldwin, 2003: Can  
668 knowledge of the state of the stratosphere be used to improve statistical forecasts of the  
669 troposphere? *Quart. J. Roy. Meteor. Soc.*, **129**, 3205–3224. doi: 10.1256/qj.02.232
- 670 Charron, M. and Coauthors, 2012: The stratospheric extension of the Canadian global  
671 deterministic medium-range weather forecasting system and its impact on tropospheric  
672 forecasts. *Mon. Wea. Rev.*, **140**, 1924-1944. doi: <http://dx.doi.org/10.1175/MWR-D-11-00097.1>.
- 674 Chipperfield, M.P., 2006: New version of the TOMCAT/SLIMCAT off-line chemical transport  
675 model. *Q. J. R. Meteorol. Soc.*, **132**, 1179-1203.
- 676 Christensen, T., B. M. Knudsen, J. P. Pommereau, G. Letrenne, A. Hertzog, F. Vial, J. Ovarlez  
677 and M. Piot, 2007: Evaluation of ECMWF ERA-40 temperature and wind in the lower  
678 tropical stratosphere since 1988 from past long-duration balloon measurements. *Atmos.*  
679 *Chem. Phys.*, **7**, 3399-3409, doi:10.5194/acp-7-3399-2007.
- 680 Dee, D. P. and Coauthors, 2011: The ERA-Interim reanalysis: configuration and  
681 performance of the data assimilation system. *Quart. J. Roy. Meteor. Soc.*, **137**, 553-597.  
682 doi: 10.1002/qj.828.
- 683 Dörnbrack A., T. Birner, A. Fix, H. Flentje, A. Meister, H. Schmid, E. V. Browell, M. J.  
684 Mahoney, 2002 : Evidence for inertia gravity waves forming polar stratospheric clouds  
685 over Scandinavia, *J. Geophys. Res.*, DOI: 10.1029/2001JD000452.
- 686 Durry, G. and A. Hauchecorne, 2005: Evidence for long-lived polar vortex air in the mid-  
687 latitude summer stratosphere from *in situ* laser diode CH<sub>4</sub> and H<sub>2</sub>O measurements. *Atmos.*  
688 *Chem. Phys.*, **5**, 1467-1472, doi:10.5194/acp-5-1467-2005.

- 689 Ern, M., P. Preusse, J. C. Gille, C. L. Hepplewhite, M. G. Mlynczak, J. M. Russell III, and M. Riese,  
690 2011: Implications for atmospheric dynamics derived from global observations of gravity wave  
691 momentum flux in stratosphere and mesosphere, *J. Geophys. Res.*, **116**, D19107,  
692 doi:10.1029/2011JD015821.
- 693 Ern, M., Q. T. Trinh, M. Kaufmann, I. Krisch, P. Preusse, J. Ungermann, Y. Zhu, J. C. Gille, M. G.  
694 Mlynczak, J. M. Russell III, M. J. Schwartz, and M. Riese, 2016: Satellite observations of middle  
695 atmosphere gravity wave absolute momentum flux and of its vertical gradient during recent  
696 stratosphere warmings, *Atmos. Chem. Phys.*, **16**, 9983-10019, doi:10.5194/acp-16-9983-2016.
- 697 Gerber, E. P. and Coauthors, 2010: Stratosphere-troposphere coupling and annular mode  
698 variability in chemistry-climate models. *J. Geophys. Res.*, **115**, D00M06,  
699 doi:10.1029/2009JD013770.
- 700 Hauchecorne, A. and M.-L. Chanin, 1980: Density and temperature profiles obtained by  
701 lidar between 35 and 70 km. *Geophys. Res. Lett.*, **7**, 565-568.  
702 doi:10.1029/GL007i008p00565
- 703 Herzog A., C. Basdevant, F. Vial, and C. R. Mechoso, 2004: The accuracy of stratospheric  
704 analyses in the northern hemisphere inferred from long-duration balloon flights. *Quart. J. Roy. Meteor. Soc.*, **130**, 607-626.
- 706 Herzog, A., C. Basdevant, and F. Vial, 2006: An Assessment of ECMWF and NCEP–NCAR  
707 Reanalyses in the southern hemisphere at the end of the presatellite era: results from the  
708 EOLE experiment (1971-72). *Mon. Wea. Rev.*, **134**, 3367-3383.  
709 doi:<http://dx.doi.org/10.1175/MWR3256.1>
- 710 Hitchcock, P., T. G. Shepherd, and G. L. Manney, 2013: Statistical characterization of Arctic  
711 polar-night jet oscillation Events. *J. Climate*, **26**, 2096-2116. doi:  
<http://dx.doi.org/10.1175/JCLI-D-12-00202.1>
- 713 Houchi, K., A. Stoffelen, G. J. Marseille and J. De Kloe, 2010: Comparison of wind and wind  
714 shear climatologies derived from high-resolution radiosondes and the ECMWF model. *J. Geophys. Res.*, **115**, D22123, doi:[10.1029/2009JD013196](http://dx.doi.org/10.1029/2009JD013196).
- 716 Huang, B., Z. Z. Hu, J. L. Kinter III, Z. Wu and A. Kumar, 2011: Connection of stratospheric  
717 QBO with global atmospheric general circulation and tropical SST. Part I: methodology and  
718 composite life cycle. *Climate Dyn.*, **38**, 1-23, doi:10.1007/s00382-011-1250-7. Huret N., F.  
719 Duruisseau and A. Andral, 2015: On the accuracy of stratospheric meteorological

720 reanalyses using wind measurements at high altitude in the stratosphere. *ESA's*  
721 *Publications Division*.

722 Huret, N., M. Pirre, A. Hauchecorne, C. Robert and V. Catoire, 2006: On the vertical  
723 structure of the stratosphere at midlatitudes during the first stage of the polar vortex  
724 formation and in the polar region in the presence of a large mesospheric descent. *J.*  
725 *Geophys. Res.*, **111**, D06111, doi:[10.1029/2005JD006102](https://doi.org/10.1029/2005JD006102).

726 Jakobson, E., T. Vihma, T. Palo, L. Jakobson, H. Keernik and J. Jaagus, 2012: Validation of  
727 atmospheric reanalyses over the central Arctic Ocean. *Geophys. Res. Lett.*, **39**, L10802,  
728 doi:[10.1029/2012GL051591](https://doi.org/10.1029/2012GL051591).

729 Kidder, S. Q. and T. H. Vonder Haar, 1995: Satellite Meteorology: An Introduction.  
730 *Academic Press*, 466 pp.

731 Knudsen B. M., T. Christensen, A. Hertzog, A. Deme, F. Vial and J.-P. Pommereau, 2006:  
732 Accuracy of analyzed temperatures, winds and trajectories in the southern hemisphere  
733 tropical and midlatitude stratosphere as compared to long-duration balloon flights.  
734 *Atmos. Chem. Phys.*, **6**, 5391-5397.

735 Knudsen, B. M., J.-P. Pommereau, A. Garnier, M. Nunes-Pinharanda, L. Denis, P. Newman,  
736 G. Letrenne and M. Durand, 2002: Accuracy of analyzed stratospheric temperatures in the  
737 winter Arctic vortex from infrared Montgolfier long-duration balloon flights 2. Results. *J.*  
738 *Geophys. Res.*, **107**(D20), doi:[10.1029/2001JD001329](https://doi.org/10.1029/2001JD001329).

739 Krishnamurti, T. N., 1959: A vertical cross section through the “polar-night” jet stream. *J.*  
740 *Geophys. Res.*, **64**(11), 1835-1844, doi:[10.1029/JZ064i011p01835](https://doi.org/10.1029/JZ064i011p01835).

741 Kuroda, Y. and K. Kodera, 2001: Variability of the polar night jet in the northern and  
742 southern hemispheres. *J. Geophys. Res.*, **106**(D18), 20703-20713,  
743 doi:[10.1029/2001JD900226](https://doi.org/10.1029/2001JD900226).

744 Kuttippurath, J. and G. Nikulin, 2012: A comparative study of the major sudden  
745 stratospheric warmings in the Arctic winters 2003/2004-2009/2010. *Atmos. Chem. Phys.*,  
746 **12**, 8115-8129.

747 Le Pichon, A., E. Blanc, and D. Drob, 2005: Probing high-altitude winds using infrasound.  
748 *J. Geophys. Res.*, **110**, D20104, doi:10.1029/2005JD006020.

- 749 Le Pichon, A. and Coauthors, 2015: Comparison of co-located independent ground-based  
750 middle atmospheric wind and temperature measurements with numerical weather  
751 prediction models. *J. Geophys. Res. Atmos.*, **120**, 8318–8331, doi:[10.1002/2015JD023273](https://doi.org/10.1002/2015JD023273).
- 752 Lehmann, E. and P. Névir, 2012: Uncertainties in relative atmospheric angular momentum  
753 computed from zonal winds in reanalysis data. *J. Geophys. Res.*, **117**, D09101,  
754 doi:[10.1029/2011JD016658](https://doi.org/10.1029/2011JD016658).
- 755 Martineau, P. and S.-W. Son, 2010: Quality of reanalysis data during stratospheric vortex  
756 weakening and intensification events. *Geophys. Res. Lett.*, **37**, L22801,  
757 doi:[10.1029/2010GL045237](https://doi.org/10.1029/2010GL045237).
- 758 Moffat-Griffin, T., R. E. Hibbins, M. J. Jarvis and S. R. Colwell, 2011: Seasonal variations of  
759 gravity wave activity in the lower stratosphere over an Antarctic Peninsula station. *J.  
760 Geophys. Res.*, **116**, D14111, doi:[10.1029/2010JD015349](https://doi.org/10.1029/2010JD015349).
- 761 Ortland, D. A., W. R. Skinner, P. B. Hays, M. D. Burrage, R. S. Lieberman, A. R. Marshall, and  
762 D. A. Gell, 1996: Measurements of stratospheric winds by the High Resolution Doppler  
763 Imager, *J. Geophys. Res.*, **101**, 10351–10363.
- 764 Podglajen, A., A. Hertzog, R. Plougonven, and N. Žagar, 2014: Assessment of the accuracy  
765 of (re)analyses in the equatorial lower stratosphere. *J. Geophys. Res. Atmos.*, **119**, 11,166–  
766 11,188, doi:[10.1002/2014JD021849](https://doi.org/10.1002/2014JD021849).
- 767 Polavarapu, S., T. G. Shepherd, Y. Rochon and S. Ren, 2005: Some challenges of middle  
768 atmosphere data assimilation. *Quart. J. Roy. Meteor. Soc.*, **131**, 3513–3527.  
769 doi:[10.1256/qj.05.87](https://doi.org/10.1256/qj.05.87).
- 770 Rivière, E. D., N. Huret, F. G.-Taupin, J.-B. Renard, M. Pirre, S. D. Eckermann, N. Larsen, T.  
771 Deshler, F. Lefèvre, S. Payan, C. Camy-Peyret et al., Role of lee waves in the formation of  
772 solid polar stratospheric clouds: Case studies from February 1997, *J. Geophys.  
773 Res.*, **105**(D5), 6845–6853, 2000. dOI: [10.1029/1999JD900908](https://doi.org/10.1029/1999JD900908)
- 774 Rüfenacht, R., N. Kämpfer and A. Murk, 2012: First middle-atmospheric zonal wind profile  
775 measurements with a new ground-based microwave Doppler-spectro-radiometer. *Atmos.  
776 Meas. Tech.*, **5**, 2647–2659, doi:[10.5194/amt-5-2647-2012](https://doi.org/10.5194/amt-5-2647-2012).

- 777 Schroeder, S., P. Preusse, M. Ern, and M. Riese, 2009: Gravity waves resolved in ECMWF  
778 and measured by SABER, *Geophys. Res. Lett.*, **36**, L10805, doi:10.1029/2008GL037054.
- 779 Sigmond, M., J. F. Scinocca, V. V. Kharin and T. G. Shepherd, 2013: Enhanced seasonal  
780 forecast skill following stratospheric sudden warmings. *Nature Geosci.*, **6**, 98-102.
- 781 Smith, F. and Coauthors, 2012: Hyperspectral Earth Observation from IASI, Five Years of  
782 Accomplishments. *Bull. Amer. Meteor. Soc.*, **93**, 347-370, doi:10.1175/BAMS-D-11-  
783 00027.1.
- 784 Straume-Lindner, A.G. and Coauthors, 2007: ADM-AEOLUS - ESA's space-borne wind  
785 profiling lidar. *Proc. 2007 EUMETSAT Meteorol. Sat. Conf.*, ISBN 92-9110-079-X,  
786 Amsterdam, The Netherlands, September, 2007.
- 787 Thompson, D. W. J., M. P. Baldwin and J. M. Wallace, 2002: Stratospheric connection to  
788 northern hemisphere wintertime weather: implications for prediction. *J. Climate*, **15**,  
789 1421-1428.
- 790 Uppala, S. M. and Coauthors, 2005: The ERA-40 re-analysis. *Q. J. R. Meteorol. Soc.* **131**,  
791 2961-3012.
- 792 Vial, F., A. Hertzog, C. R. Mechoso, C. Basdevant, P. Cocquerez, V. Dubourg and F. Nouel,  
793 2001: A study of the dynamics of the equatorial lower stratosphere by use of ultra-long-  
794 duration balloons: 1. Planetary scales. *J. Geophys. Res.*, **106**(D19), 22725–22743,  
795 doi:[10.1029/2000JD000241](https://doi.org/10.1029/2000JD000241).
- 796 Vincent, R. A. and A. Hertzog, 2014: The response of superpressure balloons to gravity  
797 wave motions. *Atmos. Meas. Tech.*, **7**, 1043-1055, doi:10.5194/amt-7-1043-2014.
- 798 Wetzel, G. and Coauthors, 2013: Validation of MIPAS-ENVISAT H<sub>2</sub>O operational data  
799 collected between July 2002 and March 2004. *Atmos. Chem. Phys.*, **13**, 5791-5811,  
800 doi:10.5194/acp-13-5791-2013.
- 801 WMO, 1995: Manual on Codes, International Codes. WMO-No. 306 (1995 edition)

802 Žagar, N., N. Gustafsson and E. Källén, 2004: Variational data assimilation in the tropics:  
803 The impact of a background-error constraint. *Quart. J. Roy. Meteor. Soc.*, **130**, 103–125.  
804 doi:10.1256/qj.03.13.

805

806

807

808

809

810

811

812

813

814

815

816

817

818

819

**Table:**

*Table 1. Statistics of ECMWF ERA-Interim/operational ECMWF data minus wind measurements for both zonal and meridional components, considering measurements retrieved from ZPB trajectories from 2000 to 2011 above Esrange and SPB trajectories obtained in the polar vortex in 2002 (Hertzog et al. 2004) respectively.*

	Zonal speed (m s <sup>-1</sup> )		Meridional speed (m s <sup>-1</sup> )	
	Polar winter 90.79-53.72 hPa	Hertzog et al. (2004)	Polar winter 90.79-53.72 hPa	Hertzog et al. (2004)
Number of points	4176	11000	4176	11000
Bias	0.1	-0.1	0.2	0.1
Standard deviation	2.6	2.3	2.5	2.2
Skewness	-0.1	0.1	-0.2	0.0
Excess kurtosis	0.8	0.0	0.5	0.1

821 **List of figures:**

822 Figure 1. Measurements of zonal (a) and meridional (b) wind velocity components  
823 between 10 km to 40 km corresponding to 200 hPa and 2 hPa. Dark blue: above Kiruna  
824 (67.9°N., 21.1°E) in December, January, February and March; light blue: above Esrange  
825 (67.9°N., 21.1°E) in June, July and August; black: above Teresina (5.1°S., 42.9°W) in 2005  
826 (easterly QBO); gray: above Teresina (5.1°S., 42.9°W) in 2008 (westerly QBO)..

827

828 Figure 2. Rolling pressure intervals considered to calculate biases. Large pressure intervals  
829 (LPI) in red and small pressure Intervals (SPI) in green. Model levels of ERA-interim data  
830 are in blue.

831

832 Figure 3. Wind biases and standard deviation as a function of pressure obtained during  
833 winter season (Dec., Jan., Feb and Mar.) above Esrange (67.9°N, 21.1°E) in red for large  
834 pressure intervals (LPI) and green for small pressure intervals (SPI), see the text section  
835 2.3 for details. a) zonal component, b) meridional component.

836 Blue horizontal lines correspond to ERA-Interim model levels.

837 Vertical black solid lines correspond to estimated uncertainty on wind component  
838 combining instrumental errors and interpolation of ECMWF data.

839

840

841

842 Figure 4. Histograms of differences between ERA-Interim and measurements above  
843 Esrange from 2000 to 2010, for the small pressure interval [90.78; 53.72] hPa at the mean  
844 pressure of 69.83 hPa.

845 a) zonal component, b) meridional component.

846

847 Figure 5. Same as Figure 3 for summer season (Jun., Jul. and Aug.) above Esrange ( $67.9^{\circ}\text{N}$ ,  
848  $21.1^{\circ}\text{E}$ ).

849

850 Figure 6. Same as Figure 3 above Teresina ( $5.1^{\circ}\text{S}$ ,  $42.9^{\circ}\text{W}$ ) in June and July 2005 (during  
851 the Easterly QBO phase).

852

853 Figure 7. Histograms of differences between the ERA-Interim reanalysis and zonal wind  
854 measurements in  $\text{ms}^{-1}$  obtained for the easterly QBO phase (those of Figure 6) at the mean  
855 pressure levels a) 9.94 hPa and b) 20.39 hPa, for LPI (red) and SPI (green).

856

Figure 8. Same as Figure 3 above Teresina ( $5.1^{\circ}\text{S}$ ,  $42.9^{\circ}\text{W}$ ) in July and August 2008 (during  
the Westerly QBO phase).

857 Figure 9. Wind biases and standard deviation as a function of pressure obtained with SPI  
858 for:

859 a) Wind speed (FF) and b) wind direction (DD) above Esrange, dark blue: Dec., Jan., Feb.,  
860 Mar.; light blue: Jun., Jul., Aug.

861 c) Wind speed (FF) and d) wind direction (DD) above Teresina, black: easterly QBO in  
862 2005; gray: westerly QBO in 2008.

863 Vertical black solid lines correspond to estimated uncertainty on wind component  
864 combining instrumental errors and interpolation of ECMWF data.

865

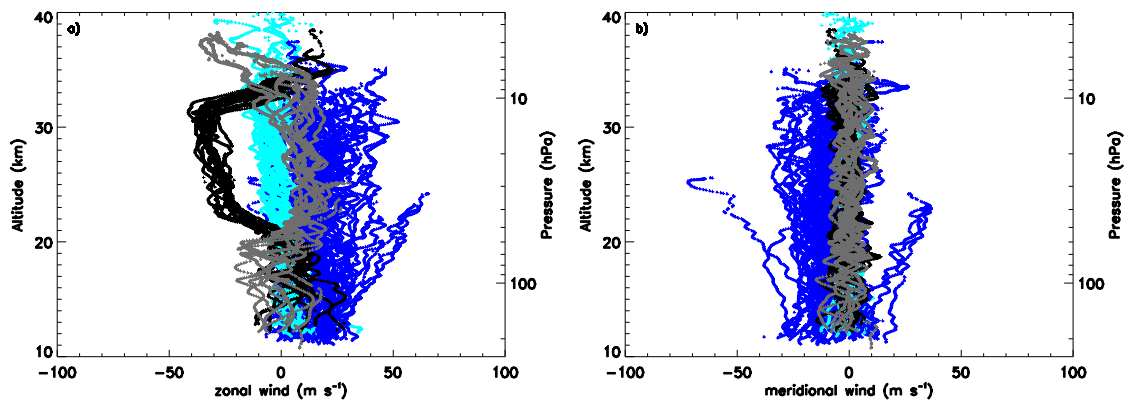


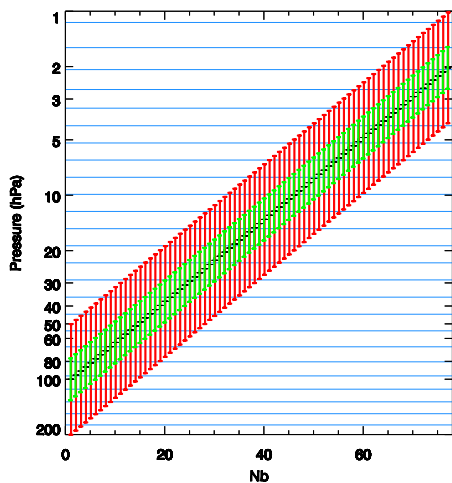
Figure 1. Measurements of zonal (a) and meridional (b) wind velocity components between 10 km to 40 km corresponding to 200 hPa and 2 hPa.

Dark blue: above Esrange (67.9°N., 21.1°E) in December, January, February and March.

Light blue: above Esrange (67.9°N., 21.1°E) in June, July and August.

Black: above Teresina (5.1°S., 42.9°W) in 2005 (easterly QBO).

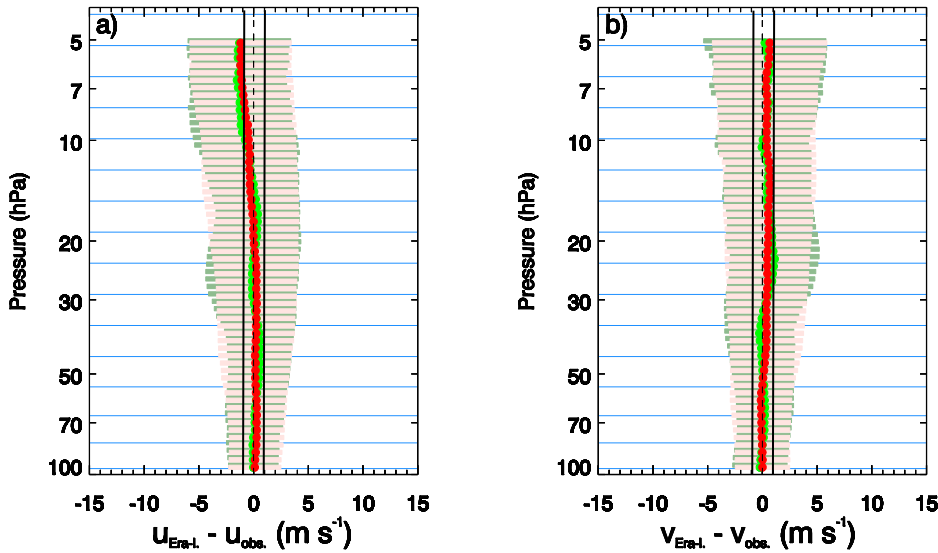
Gray: above Teresina (5.1°S., 42.9°W) in 2008 (westerly QBO).



867

868 Figure 2. Rolling pressure intervals considered to calculate biases. Large pressure intervals  
869 (LPI) in red and small pressure intervals (SPI) in green. ERA-interim levels are shown in  
870 blue.

871



872  
 873 Figure 3. Wind biases and standard deviation as a function of pressure obtained during  
 874 the winter season (Dec., Jan., Feb. and Mar.) above Esrange ( $67.9^{\circ}\text{N}$ ,  $21.1^{\circ}\text{E}$ ) in red for  
 875 large pressure intervals (LPI) and green for small pressure intervals (SPI), see the text  
 876 (section 2.3) for details.

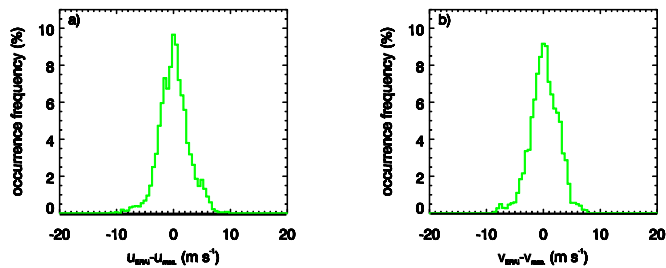
877       a) zonal component, b) meridional component.

878 Blue horizontal lines correspond to ERA-Interim levels.

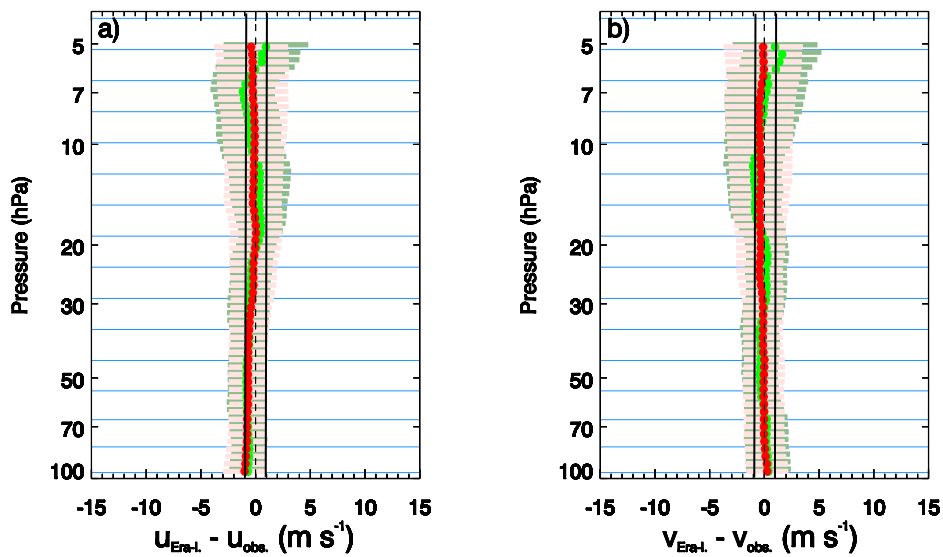
879 Vertical black solid lines correspond to estimated uncertainty on the wind component  
 880 combining instrumental errors and interpolation of ECMWF data.

881

882



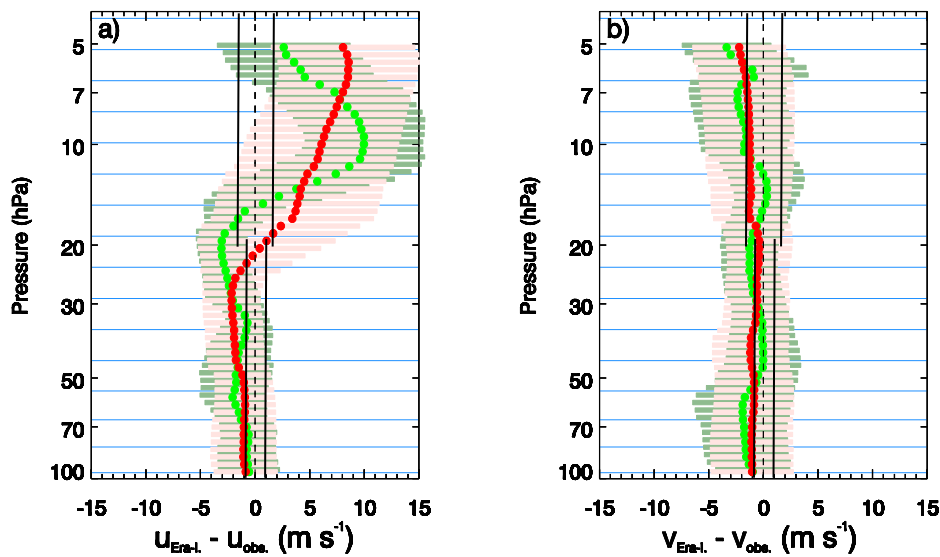
883 Figure 4. Histograms of differences between ERA-Interim and measurements above  
884 Esrange from 2000 to 2010, for the small pressure interval [90.78; 53.72] hPa at the mean  
885 pressure of 69.83 hPa.  
886 a) zonal component, b) meridional component.  
887



888

889 Figure 5. Same as Figure 3 for the summer season (Jun., Jul. and Aug.) above Esrange  
 890 (67.9°N, 21.1°E).

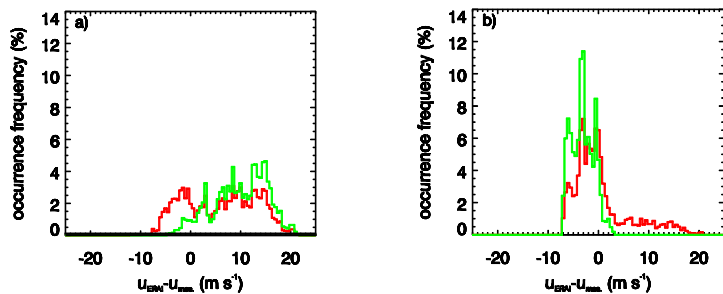
891



892     Figure 6. Same as Figure 3 above Teresina ( $5.1^{\circ}\text{S}$ ,  $42.9^{\circ}\text{W}$ ) in June and July 2005 (during  
 893     the Easterly QBO phase).

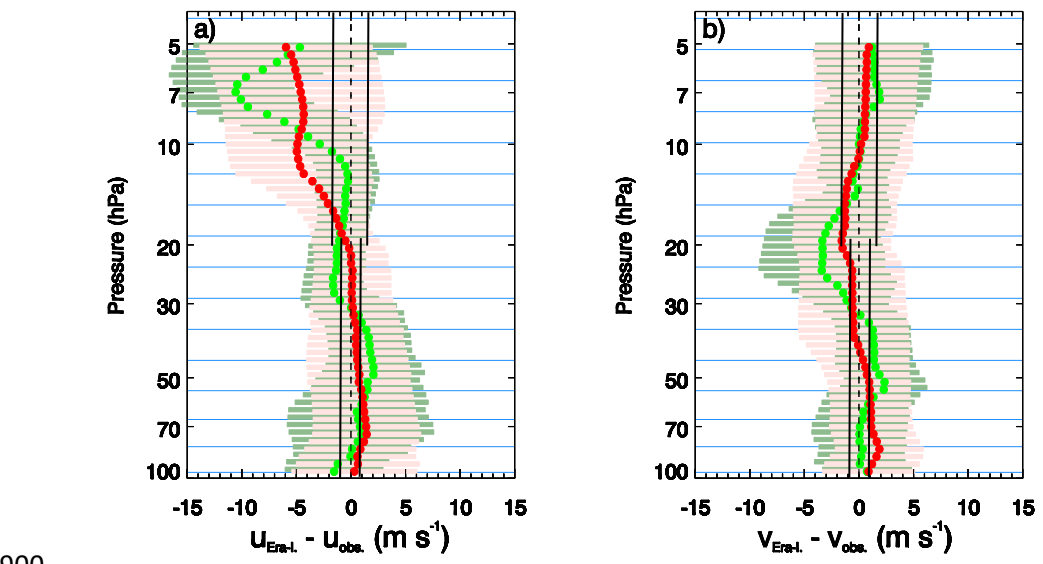
894

895



896 Figure 7. Histograms of differences between the ERA-Interim reanalysis and zonal wind  
897 measurements in  $\text{m s}^{-1}$  obtained for the easterly QBO phase (those of Figure 6) at the mean  
898 pressure levels a) 9.94 hPa and b) 20.39 hPa, for LPI (red) and SPI (green).

899

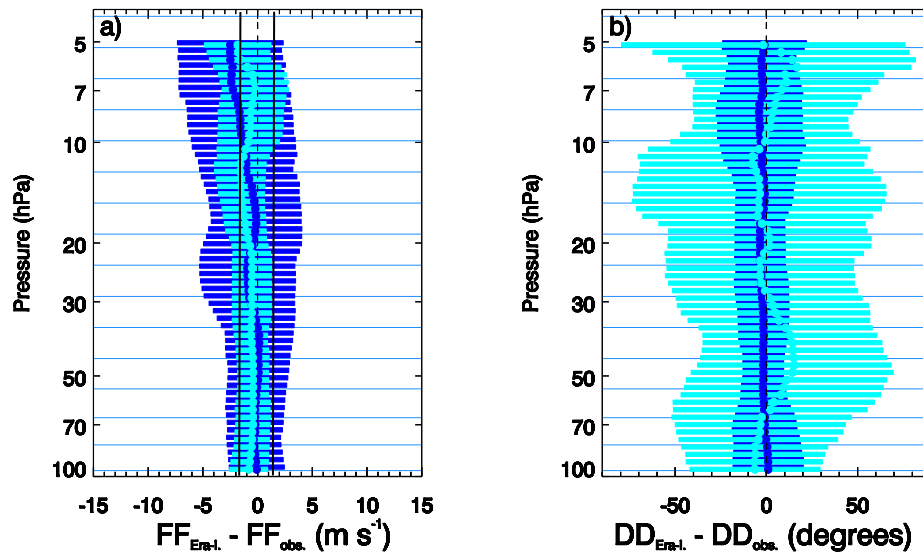


900

901    Figure 8. Same as Figure 3 above Teresina (5.1°S, 42.9°W) in July and August 2008 (during  
 902    the Westerly QBO phase).

903

904



905

Figure 9. Wind biases and standard deviation as a function of pressure obtained with SPI for:  
 a) Wind speed (FF) and b) wind direction (DD) above Esrange, dark blue: Dec., Jan., Feb., Mar.; light blue: Jun., Jul., Aug.  
 c) Wind speed (FF) and d) wind direction (DD) above Teresina, black: easterly QBO in 2005; gray: westerly QBO in 2008.  
 Vertical black solid lines correspond to estimated uncertainty on wind component combining instrumental errors and interpolation of ECMWF data.